Dalton Transactions

PAPER

View Article Online
View Journal | View Issue

Cite this: *Dalton Trans.*, 2016, **45**, 7605

Synthesis of oxime-based CO-releasing molecules, CORMs and their immobilization on maghemite nanoparticles for magnetic-field induced CO release†

Hajo Meyer,[a] Markus Brenner,[a] Simon-P. Höfert,[a] Tim-O. Knedel,[a] Peter C. Kunz,[a] Annette M. Schmidt,[b] Alexandra Hamacher,[c] Matthias U. Kassack[c] and Christoph Janiak*[a]

Received 15th December 2015,
Accepted 20th March 2016

DOI: 10.1039/c5dt04888e

www.rsc.org/dalton

Oxime-based CO-releasing molecules (oximeCORMs) were immobilized with a catechol-modified backbone on maghemite iron oxide nanoparticles (IONPs) to give oximeCORM@IONP. The CO release from the free and immobilized oximeCORMs was measured using the standard myoglobin assay. The oximeCORM-nanoparticles were coated with dextran for improved water solubility and confined into an alginate shell for protection and separation from the surrounding myoglobin assay to allow for CO release studies by UV/Vis absorption without interference from highly-absorptive oximeCORM@IONP. Half-lifes of the oxime-based polymer-confined alginate@dextran@oximeCORM@IONPs were estimated at 20 °C to 814 ± 23 min, at 37 °C to 346 ± 83 min and at 50 °C to 73 ± 1 min. The alginate@dextran@oximeCORM@IONP composite showed a further decrease of the half-life of CO release to 153 ± 27 min at 37 °C through local magnetic heating of the susceptible iron oxide nanoparticles with application of an external alternating magnetic field (31.7 kA m^{-1}, 247 kHz, 39.9 mTesla). The activation energy for the CO release from molecular dicarbonylchlorido(imidazole-2-carbaldehydeoxime)(alkoxycarbonyl)ruthenium(II) complexes is determined to be ~100 kJ mol^{-1} for five different imidazole-oxime derivatives.

Introduction

The toxic physiological effects of carbon monoxide (CO) were first described by John Haldane in 1927.[1] CO is generally known as a highly toxic gas which hinders the oxygen transport in the blood system, by strong coordination to the oxygen binding site in hemoglobin. Even breathing of small quantities (about 100 ppm in air) of this color- and odorless gas can be potentially harmful to the human organism.[2,3] On the other hand, carbon monoxide is classified as a biochemical messenger molecule like hydrogen sulfide and nitrogen oxide.[4–6] Human organisms express *heme oxygenase* enzymes,[7] which are capable of producing carbon monoxide continuously in order to regulate the circadian rhythms, memory and hemodynamics.[8–10] Due to its regulatory and cytoprotective effects CO has already been extensively investigated for medical applications.[9] Yet, when CO is administered to a human organism as a gas, it is difficult to accumulate at a specific site (*e.g.* tumor or burned skin). Gaseous CO as a therapeutic agent features a half-life of 3 to 7 hours in the body and was well tolerated at 3 mg per kg for one hour. CO binds reversibly to cellular targets and the only way for CO to exit mammal bodies in a therapeutic approach was by lung exhalation.[11,12] In fact the gas also reaches healthy tissue and the dose needs to be relatively high in order to achieve an effect on the desired tissue. In addition, the quantity needs to be carefully controlled and special administering equipment is necessary.

CO releasing molecules (CORMs), primarily metal carbonyl derivatives were invented for specific targeting and controlled release of carbon monoxide. Metal carbonyl derivatives are investigated also as antibacterial compounds and for their anticancer therapeutic potential.[13] However, the first CORMs were hardly water-soluble and released CO a way too fast for precise administering (half the gas load in less than one minute under physiological conditions).[14] Motterlini and co-

[a]*Institut für Anorganische Chemie und Strukturchemie, Universität Düsseldorf, 40204 Düsseldorf, Germany. E-mail: janiak@uni-duesseldorf.de*
[b]*Institut für Physikalische Chemie, Universität zu Köln, Luxemburger Str. 116, D-50939 Köln, Germany. E-mail: annette.schmidt@uni-koeln.de*
[c]*Institut für Pharmazeutische und Medizinische Chemie, Universität Düsseldorf, 40204 Düsseldorf, Germany. E-mail: matthias.kassack@hhu.de*

†Electronic supplementary information (ESI) available: Synthesis for oxime-based CORMs, NMR, IR and ESI-mass spectra, myoglobin assay, leaching experiments, DLS experiments, TEM measurements, toxicity tests, and activation energy. See DOI: 10.1039/c5dt04888e

workers[3,15] introduced in 2003 the water-soluble complex [Ru(CO)$_3$(glycinate)] (CORM-3) which released CO under physiological conditions[16] and showed vasodilatative, anti-inflammatory, renoprotective and anti-apoptosis effects in preclinical studies.[17] Since the last decade, Ru-based CORMs have become a very important field of research with several studies of CORM-2 and the water-soluble CORM-3 (Scheme 1).[9,14,16]

The half-life of CO release from CORM-3 *via* a pseudo-first-order reaction is 1 min at 37 °C in PBS buffer,[18] 2.3 min at 30 °C in PBS buffer[19] and 3.6 min in human plasma,[20] apparently due to CO-abstraction by heme proteins.[21] Recent studies presented CORMs which liberate CO upon external stimuli like change in the pH,[22,23] increasing temperature, UV irradiation[24,25] and oxidative or enzymatic degradation.[26,27] The immobilization of CORMs in[28] and on[29,30] other materials opens new methodologies in medicinal chemistry.[31,32] However, different possible medical applications of CORMs will require CORMs with different release kinetics.

Drugs which are conjugated to polymers are restricted to the vascular system and can be transported directly to the target area. A passive accumulation of macromolecular systems in tumor tissues due to the so-called enhanced permeability and retention (EPR) effect was first described and investigated by Maeda *et al.*[33,34]

The growth of tumors (>2 mm) is ensured by fast growing blood vessels to supply nutrients and dioxygen. The blood vessels are destabilized due to vascular endothelial growth factors (VEGFs) into the extracellular space and have higher permeability than normal grown blood vessels.[35] The resulting blood vessels lack tight junctions that are normally present between adjacent vascular endothelial cells. This deficiency leaves holes on an order of magnitude greater than normal vascular pores (healthy tissue has pores of 5 to 8 nm, tumor tissue can have pores of about 50 nm and inter-endothelial junctions of about 500 nm). The EPR effect refers to the properties of these large pores to allow polymers to enter the tumor interstitium and to remain and accumulate there because the polymers are not removed by the lymphatic system.[36]

The accumulation of functionalized polymers in tumor tissue with the ability to release CO is an additional concept of developing polymer–CORM conjugates. In such conjugates the use of a slow CO releaser from which the CO release can be triggered or activated by magnetic heating through alternating magnetic field should be of interest.

Different CORMs with ruthenium carbonyls are known and the number is still increasing.[37] Oresmaa *et al.* described a simple synthetic route to oxime-based CORMs for which they reported a longer half-life for CO release than for CORM-3 [38] (Scheme 1).

In our previous work, we presented a new concept of controlled CO release by covalently attaching the CO-releasing molecule (a CORM-3 analogue) to the surface of iron oxide nanoparticles which are susceptible to local heating through an external alternating current magnetic field.[39] The increased temperature of the nanoparticles, due to the external alternating magnetic field, decreased the half-life from 13 ± 2 min to 7 ± 2 min in a buffered myoglobin-assay solution kept at 25 °C.

Here we target the covalent immobilization of relatively stable (long half-life) oxime-based CORMs on the surface of iron oxide nanoparticles. In addition a dextran coating is applied for better water solubility and as a barrier against heme proteins.

At the same time the strong absorptivity of the black IONP dispersion hampers CO release studies with the standard myoglobin assay in the same dispersion. The CO release by a myoglobin assay is followed by UV/Vis spectrometry. Therefore, we used an alginate confinement of "water-soluble" dextran@oximeCORM@IONP to achieve a spatial separation from the surrounding myoglobin assay.

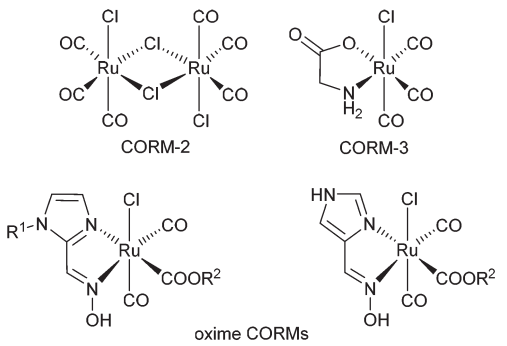

Scheme 1 Scheme of the synthesized oxime-based CORMs from Oresmaa *et al.* with their half-lifes. The half-lifes were determined at ambient (room) temperature in a phosphate buffered saline solution (pH = 6.8).[38]

Results and discussion

Synthesis

The covalent immobilization of the oxime-based CORMs on an iron oxide nanoparticle (IONP) surface is depicted in Scheme 2.

Starting with the commercially available 2-chloro-3′,4′-dihydroxyacetophenone **3** (Scheme 3), we first tried unsuccessfully a simple condensation reaction with 1*H*-imidazole-2-carbaldehyde **4** to try to obtain the condensation product

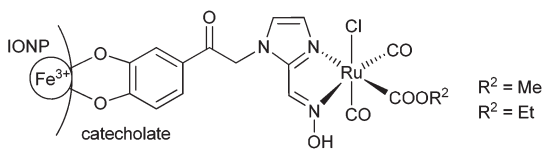

Scheme 2 Covalent immobilization of oxime-based CORM on an iron oxide nanoparticle (IONP) surface through a catecholate group.

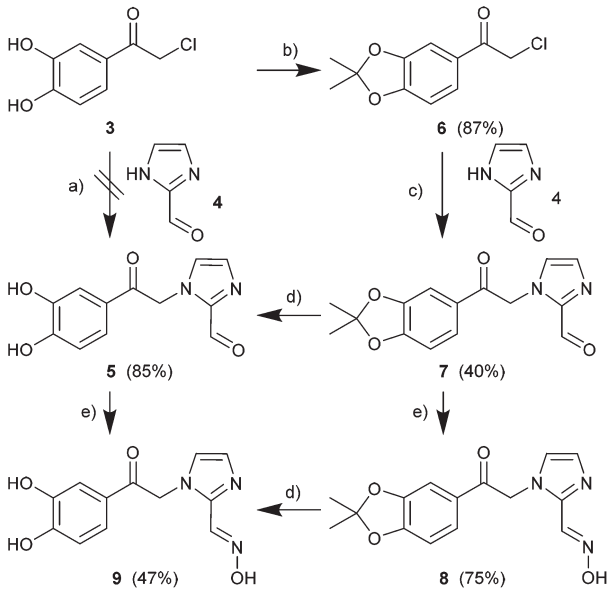

Scheme 3 Synthetic route (with yields) for the coupling of the catechol group with 1*H*-imidazol-2-carbaldehyde (**4**) to 1-(2-(3,4-dihydroxyphenyl)-2-oxoethyl)-1*H*-imidazole-2-carbaldehyde (**5**) and the acetate protected (**8**) and unprotected oxime (**9**). (a) Acetonitrile, sodium carbonate, 60 °C, 5 d; (b) dry toluene, dry acetone, phosphorus pentoxide, 75 °C, 4 h; (c) acetonitrile, sodium carbonate, 60 °C, 7 d; (d) acetic acid, hydrochloric acid, 100 °C, 2 h; (e) sodium carbonate, hydroxylammonium chloride, 70 °C, 24 h.

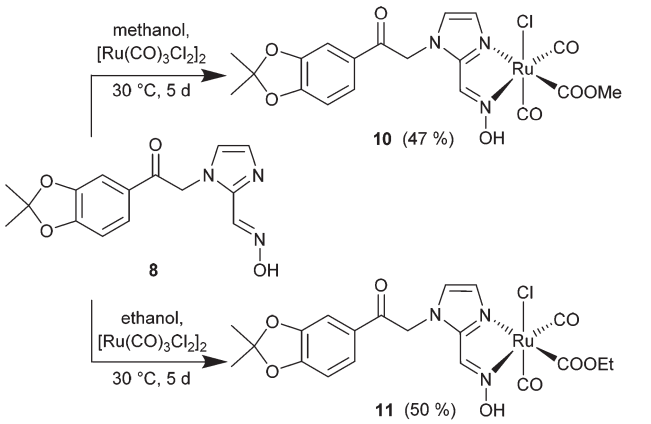

Scheme 4 Synthesis of CORMs with the diol-protected catechol oxime **8** as methoxy- (**10**) and ethoxy- (**11**) ruthenium complexes (yields in parentheses).

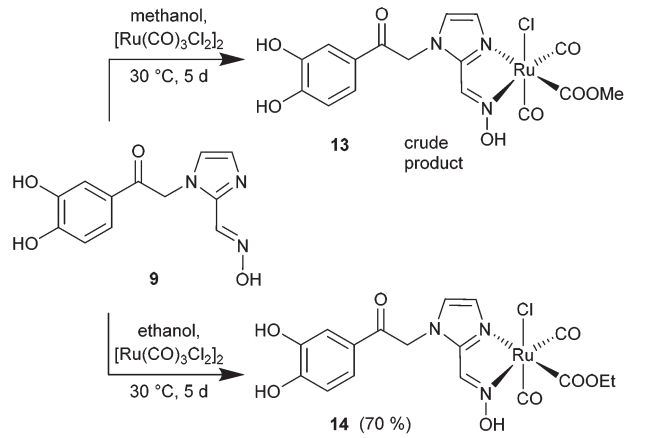

Scheme 5 Synthesis of CORMs with the (unprotected) catechol oxime **9** as methoxy- (**13**) and ethoxy- (**14**) ruthenium complexes (yields in parentheses).

1-(2-(3,4-dihydroxyphenyl)-2-oxoethyl)-1*H*-imidazole-2-carbaldehyde **5** in a single step. The single-step route failed so that the diol was first protected by an acetal group to form product **6** in good yields. The condensation of **6** with **4** to give 1-(2-(3,4-dihydroxyphenyl)-2-oxoethyl)-1*H*-imidazole-2-carbaldehyde **7** in acetonitrile with an equimolar ratio of a base proved successful. Acid cleavage of the acetal protecting group afforded the desired product 1-(2-(3,4-dihydroxyphenyl)-2-oxoethyl)-1*H*-imidazole-2-carbaldehyde **5** in high yields. Introducing the oxime function into compounds **7** and **5** was done similarly to ref. 38 (Scheme 3). The reaction times were extended up to 24 h to obtain good yields for (*E*)-1-(2-(2,2-dimethylbenzo[*d*]-[1,3]dioxol-5-yl)-2-oxoethyl)-1*H*-imidazol-2-carbaldehyde-oxime **8** (75%) and 1-(2-(3,4-dihydroxyphenyl)-2-oxoethyl)-1*H*-imidazole-2-carbaldehyde-oxime **9** (47%).

The synthesis of the diol-protected ruthenium carbonyl oximes **10** and **11** was performed as described in the literature[38] with $[Ru(CO)_3Cl_2]_2$ (**12**) and an extended reaction time of 5 d (Scheme 4). To obtain the methoxy-compound **10** the reaction was carried out in methanol and for the ethoxy-compound **11** in ethanol. CORMs **10** and **11** precipitated from the solution as the modified backbone leads to lower solubility in polar solvents than for the parent compounds **a** and **b** (Scheme 1).

For immobilization on an iron oxide nanoparticle surface the dihydroxyphenyl-oxime **9** was reacted with $[Ru(CO)_3Cl_2]_2$ (**12**) to give the ruthenium carbonyl oximes **13** and **14** as shown in Scheme 5.

Electron spray ionization mass spectrometric analysis of **10–14** in acetonitrile solution showed ligand lability (see Fig. S3, ESI†). For compounds **10** and **11** or **13** and **14**, respectively, identical mass spectra were obtained and the isotopic pattern showed a ruthenium complex from which the methoxy (or ethoxy) group (OR^-), a CO unit and/or a chloride ligand had been lost. In addition, a proton was abstracted, presumably from the N–OH group, which together with CO and OR^- amounts to the liberation of formic acid ester or with OR^- only to the liberation of the alcohol ROH. Instead, acetonitrile was coordinated under ESI-MS conditions. Hence, the dominant fragments (for ^{102}Ru) of m/z = 499.1 (**10**, **11**) or 459.2 (**13**, **14**) correspond to $[M - OR^- - CO - Cl^- - H^+ + CH_3CN]^+$ and m/z = 527.0 (**10**, **11**) or 487.0 (**13**, **14**) to $[M - OR^- - Cl^- - H^+ + CH_3CN]^+$ (R = Me, Et). The lability of carbonyl complexes in ESI mass spectrometric analysis is known.[40]

IR spectroscopic measurements of **10–14** show the expected strong carbonyl absorptions (Fig. S1 in the ESI†) which agree

Table 1 Carbonyl stretching frequencies of oxime ruthenium CORMs[a]

Compound	νCO [cm^{-1}]	νCO [cm^{-1}]	Ref.[d]
1a[a,c]	2064	1990	Fig. S2-1a
2a[a,c]	2067	1994	Fig. S2-1a
1a[b,c], **2a**[b,c]	2056–2059	1980–1985	38
10[a]	2075	1989	Fig. S2-1b
11[a]	2065	1988	Fig. S2-1b
14[a]	2077	2012	Fig. S2-2
17[a]	2064	1995, 1961[e]	Fig. S2-3
18[a]	2061	1991	Fig. S24
18[a] after CO release	2071, 2015	1992	Fig. S24

[a] KBr disks. [b] FT-IR in DMSO. [c] Formula in Scheme 1. [d] This work with reference to the figure showing the IR spectrum, unless indicated otherwise. [e] We trace the third CO band to partial CO release during CORM deposition on IONP and inclusion in dextran in water (*cf.* Scheme 6).

well with the ones reported by Oresmaa *et al.*[38] for **a** and **b** in the regions 2056–2059 cm^{-1} and 1980–1985 cm^{-1} (Table 1).

Maghemite nanoparticles (**15**) were synthesized by the known method from Ewijk *et al.*[41] A catechol based anchor group is common for immobilizing molecules on an IONP surface.[42] The unprotected catechol–oxime ruthenium complex **14** was immobilized on the surface of maghemite nanoparticles. Compound **14** was dissolved in water under basic conditions and stirred with maghemite nanoparticles. To prevent agglomeration of the nanoparticles the combined solutions of both compounds were kept below pH 8. After precipitation with acetone and washing with ethanol, the oximeCORM@IONP composite nanoparticles **16** were not able to build a stable dispersion in MOPS-buffer or water but sedimented within a few seconds (see the ESI† for DLS and TEM analysis of **16**). To increase the solubility of the oximeCORM@IONP nanoparticles in water, they were coated by using dextran polymers to give dextran@oximeCORM@IONP (**17**). Water-soluble dextran (M = 500 000 g mol^{-1}) consists of glucose monomers with α-1,4- and α-1,6-connectivity and was added during the reaction of **14** with the iron oxide nanoparticles.

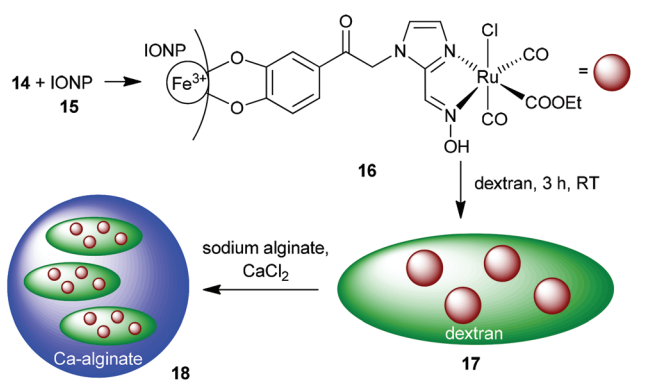

Scheme 6 Synthesis of the composite material alginate@dextran@oximeCORM@IONP (**18**) by immobilization of the oximeCORM **14** on the maghemite nanoparticle surface **15**.

The IR spectrum of the composite material **17** (Fig. S4 in the ESI†) shows the OH-vibrations of the dextran at 3600–3000 cm^{-1} and the carbonyl region exhibits three strong absorptions at 2064, 1995 and 1961 cm^{-1}.

The amount of ruthenium in the dextran@oximeCORM@IONP (**17**) composite was determined by atomic absorption spectroscopy (AAS) to an average of 0.60 wt% ruthenium and a molar Ru : Fe ratio of 1 : 25 (see Experimental section or the ESI† for details). This is the same molar Ru : Fe ratio as in our previous report on a CORM-3 analog on IONP (Ru : Fe 1 : 25[39]).

Further, composite **17** was incorporated into calcium alginate spheres. A mixture of **17** with sodium alginate was added dropwise to a calcium chloride solution. Calcium cross-linked alginate spheres were rapidly formed which almost quantitatively incorporate the dextran@oximeCORM@IONP substrate as is evident from the clear, non-colored surrounding solution (Fig. S26 in the ESI†). The IR spectrum of the composite material **18** (Fig. S28 in the ESI†) shows two strong absorptions at 2061 and 1991 cm^{-1}, which are indicators for the immobilized carbonyls on the nanoparticle surface. Yet, the still necessary use of water to anchor **14** on IONPs to give **16** and in the dextran and alginate coating of **16** to **17** and further to **18** represents a drawback and already induces partial decomposition with a loss of CO (see below and Table S1 in the ESI†). Future work has to address replacing water by other solvents.

CO release

The half-lifes $t_{1/2}$ of the CO release from compounds **1**, **2**, **10**, **11** and **18** were measured using the myoglobin assay to elucidate differences in the CO release kinetics at 20, 37 and 50 °C (Fig. 1a). A 3-(*N*-morpholino)propanesulfonic acid buffer

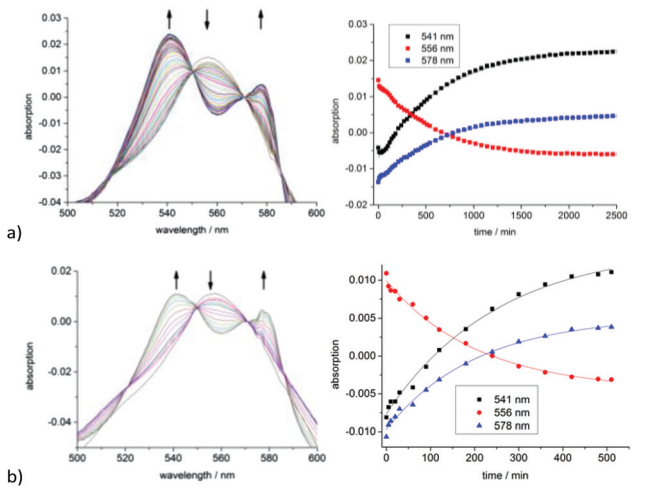

Fig. 1 Time-dependent visible absorption spectra (left) and the plot of the intensity changes of selected wavelengths (right) of alginate@dextran@oximeCORM@IONP (**18**) with the myoglobin assay at 37 °C (a) without the influence of an external alternating magnetic (AC) field to $t_{1/2}$ = 346 ± 83 min, and (b) with alternating field $t_{1/2}$ = 155 ± 27 min. Arrows in the absorption spectra mark the selected wavelengths with the direction of their time-dependent change.

(pH = 7.4, 0.1 M) was used by us instead of the phosphate buffer which Oresmaa *et al.* described to prevent further agglomeration of the IONP-containing samples and to make the results comparable to our previously presented system.[39] All measurements were done three times to ensure reproducibility.

The half-lifes of the CO release are listed in Table 2 (for kinetic data see Fig. S5–S25 in the ESI†). Oresmaa *et al.* described a slightly faster CO release from the methoxy-**1a** ($t_{1/2}$ = 60 min) than from the ethoxy-**2a** oximeCORM (*cf.* Scheme 1) ($t_{1/2}$ = 70 min) at ambient temperature, albeit not further specified temperature.[38] From our thermostated measurement at 20 °C, 37 °C and 50 °C, the methoxy- (**1a**) and ethoxy- (**2a**) derivatives have the same half-life within the experimental error. We note that the oximeCORM compounds **1a** and **2a** show a slower CO release than CORM-3 at 37 °C ($t_{1/2} \leq 1$ min) in the presence of the myoglobin assay.

The diol-protected catechol oximeCORMs **10**, **11** and the unprotected catechol oximeCORM **14** also show similar half-lifes within the experimental error with a slightly faster release than from **1a** and **2a** at 20 °C, which might correlate to the modified backbone.

The dark "soluble" dextran-coated iron oxide nanoparticles **17** do not lend themselves to follow the CO release with the myoglobin assay due to their strong UV/Vis absorption.[42] Dextran coating leads to a stable dispersion with no sedimentation anymore. Thus, the high background absorption from the dark color from the iron oxide nanoparticles masks the absorption changes of the myoglobin assay. The confinement of dextran@oximeCORM@IONP in calcium alginate spheres allowed for minimization of the spectral interference by separation within the myoglobin assay.[42] We briefly note that there are other methods available for CO release studies from CORMs. Electrochemical sensing,[43] fluorescent probes,[44,45] gas-phase IR spectroscopy,[43] or gas chromatography[46,47] have been reported in the literature. Yet, the inexpensive and easy alginate-separation method allows for working with the widely accepted myoglobin assay.

The calcium alginate shell around the "soluble" dextran-coated iron oxide nanoparticles presents a membrane, which allows for diffusion of gaseous CO but prevents the interaction with the outside protein and sodium dithionite of the myoglobin assay.[42]

Previous CO-release studies from CORM-2 and CORM-3 showed that the rate depended on myoglobin and was accelerated by an increasing concentration of the reducing agent, sodium dithionite.[21] The loss of carbon monoxide was shown when CORM-3 was preincubated with sodium dithionite in the absence of myoglobin. After reduction of the myoglobin and removal of the sodium dithionite in the assay, no liberation of CO from CORM-3 was seen.[19] The interactions of CORM-3 with proteins result in the loss of a chloride ion, glycinate, and one CO ligand because of rapid formation of stable protein–Ru (CO_2) adducts.[21]

For the oxime-based CORMs (**1**, **2**) Oresmaa suggested "that the alkoxycarbonyl group plays an important role in CO release. Whether the role is merely to destabilize carbonyl ligands or act as a source of CO remains to be studied".[38]

Furthermore, the alginate spheres containing the iron oxide nanoparticles were magnetic and could be retained at the bottom of the cuvette with a magnet to prevent them from moving into the light path during UV/Vis measurement (Fig. S22 in the ESI†). Spheres of the composite material **18** were transferred within 30 min after their synthesis into the cuvette under nitrogen to avoid contamination with dioxygen. MOPS-buffer and myoglobin solution (containing $Na_2S_2O_3$) were added and the CO release measurements were started immediately by collecting time-dependent UV/Vis spectra at 20, 37 and 50 °C. The half-lifes were determined from the kinetic curves of the absorption changes with time (see the ESI†) and are listed in Table 2.

The CO release of the composite material **18** was also measured at 37 °C (surrounding solution temperature) under the influence of an external alternating magnetic (AC) field

Table 2 Half-lifes of the CO release from oximeCORMs determined using the myoglobin assay at different temperatures

	$t_{1/2}$ [min]			
Compound	20 °C	~25 °C	37 °C	50 °C
1a	220 ± 23		21 ± 2	5 ± 1
1a[a]		60		
2a	226 ± 9		18 ± 1	6 ± 1
2a[a]		70		
10	172 ± 23		18 ± 3	4 ± 1
11	155 ± 13		18 ± 1	4 ± 1
14	207 ± 6		16 ± 1	3 ± 1
18	814 ± 23		346 ± 83	73 ± 1
18 in AC field[b]			153 ± 27	

[a] The work of Oresmaa *et al.*[38] does not specify a temperature. Thus, ambient or room temperature can be assumed which can be – depending on season, climate and weather – somewhere between 15 °C to 30 °C. The half-life values from Oresmaa *et al.* must be traced to a temperature higher than 20 °C or to buffer influences. [b] With applied alternating magnetic field (31.7 kA m^{-1}, 247 kHz, 39.9 mTesla).

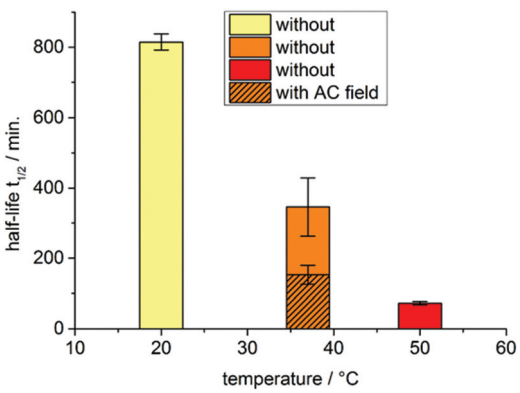

Fig. 2 Half-lifes for temperature-dependent CO release from alginate@dextran@oximeCORM@IONP (**18**) without and with applied alternating (AC) magnetic field (at 37 °C only).

(31.7 kA m^{-1}, 247 kHz, 39.9 mTesla) to determine the accelerated CO release due to magnetic heating of the iron oxide particles (Fig. 2). The estimated half-life at 37 °C with an AC field is 153 ± 27 min (ESI, Fig. S27†). The magnetic heating of the maghemite nanoparticles leads to an accelerated CO release by a factor 2.3 through the increase in the surface temperature of the IONP, which affects the attached CORM (Fig. 3a).

We determined the AC effect only at the physiologically relevant temperature of 37 °C. We have shown recently with a CORM-3@IONP analog that the CO-release is accelerated from a half-life of 890 ± 70 min at 20 °C, 172 ± 27 min at 37 °C and 45 ± 7 min at 50 °C with an AC field to 155 ± 18 min at 20 °C, 65 ± 5 min at 37 °C and 30 ± 3 min at 50 °C.[42] Thus, the acceleration of CO release or lowering of the CORM half-life by the AC field will be even larger at 20 °C.

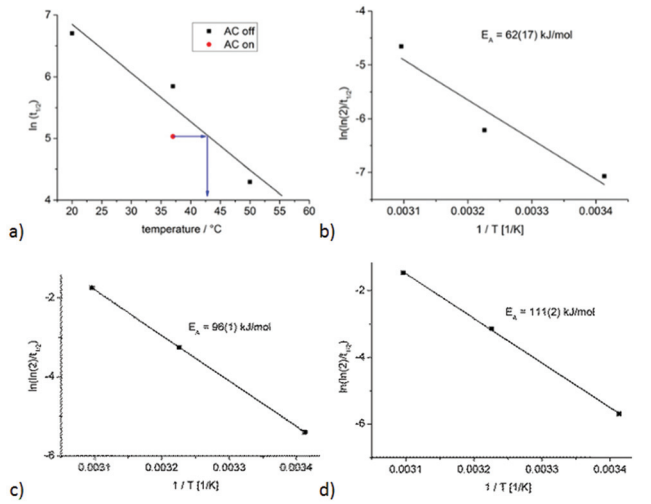

Fig. 3 (a) Correlation of $\ln(t_{1/2})$ *versus* the temperature for **18** for AC on and off to estimate the IONP surface temperature upon magnetic heating, thereby assuming a direct correlation between their half-life and temperature. The initial temperature position of the red dot (AC on) is the set solution temperature. The AC field then increases the temperature on the IONP surface as traced by the blue arrows. (b–d) Arrhenius plots for **18** (b), **11** (c) and **14** (d) of $\ln k = \ln(\ln(2)/t_{1/2})$ *versus* $1/T_{Kelvin}$ to determine the activation energy from the slope ($-E_A/R$, R = 8.314 J mol^{-1} K^{-1}) of the graph.

IR spectroscopic measurements showed shifted carbonyl absorptions after the CO release of the composite material alginate@dextran@oximeCORM@IONP (**18**) from 2061 and 1991 cm^{-1} to 2071, 2015 and 1992 cm^{-1} (ESI, Fig. S28†). The complete disappearance of the carbonyl absorption bands could not be observed after the CO release studies with the myoglobin assay. Therefore, the release of both CO-ligands from oximeCORMs does not take place. For CORM-3 only one mol of CO can be released from $[Ru(CO)_3Cl(O_2CCH_2NH_2)]$ in PBS buffered solution with myoglobin. After the release of one CO from CORM-3 an inactive form, termed iCORM is formed. The inactive iCORM-form of CORM-3 is not able to release further CO after the loss of one CO.[16]

The absolute amount of released CO was determined with the Lambert–Beer law and gave the formation of 0.2(1) mol carbon monoxide per mol of Ru from alginate@dextran@oximeCORM@IONP (**18**), 0.9(1) mol for **10**, 0.8(1) mol for **11** and 0.9(1) mol for **14** in the myoglobin assay (see eqn (1) in the ESI†). The low CO amount per Ru in **18** results apparently from the CO loss during the synthesis. It is known from recent work that CORM-2 ($[Ru(CO)_3Cl_2]_2$) will lose 1.8 CO equivalents as CO_2 in water within 24 h.[37] In order to anchor **14** on maghemite nanoparticles (**15**) and coat with dextran to yield dextran@oximeCORM@IONP (**17**), the mixture had to be stirred in water for 3 h. Inclusion of **17** in the alginate spheres, giving **18** added another ~35 min of water contact before the CO release measurements. Attempts to replace water by methanol in the formation of **17** led to agglomeration of the IONPs.

In our previous work on a CORM-3@IONP analog we realized that $\ln(t_{1/2})$ shows a linear correlation with temperature and that the $\ln(t_{1/2})$ values at 37 °C (AC off) and 20 °C (solution

Table 3 Cytotoxicity test of ruthenium CORMs and cisplatin against the human ovarian cancer cell line A2780, the human tongue cancer cell line Cal27 and the non-cancer cell line HEK293. The inhibition of cell growth is expressed as % of untreated control[a]

	Cell line					
	A2780		Cal27		HEK293	
	Concentration/μmol L^{-1}					
Compound	100	10	100	10	100	10
Cisplatin	93.2	—	95.2	—	94.3	—
CORM-2	0	0	20.8	0	13.9	9.23
CORM-3	5.20	5.73	22.0	2.25	18.0	7.04
14[b]	12.7	3.07	29.3	2.65	33.9	0
	Concentration/μg mL^{-1}					
	100	10	100	10	100	10
Dextran@oxime-CORM@IONP (**17**)	0	0	0	0	0	0

[a] Growth inhibition values are the average of experiments performed in triplicate. [b] See Scheme 5 for the formula of the ethoxy-oximeCORM **14**.

temperature, AC on) were very close, with ln(172) = 5.15 and ln (155), respectively = 5.04. From this, we deduced that the AC field at 20 °C generates an IONP surface temperature of about 37 °C.[42] The surface temperature of the IONP through the AC field was determined through a plot of $\ln(t_{1/2})$ *versus* the temperature (Fig. 3a). Under the assumption that the half-life for the same material is only a function of temperature, then the $\ln(t_{1/2})$ value reached under the AC magnetic field would correlate with an IONP surface temperature of 43 °C in the surrounding solution temperature of 37 °C (Fig. 3a). A determination of the activation energy E_A for the CO release from the alginate composite material **18** with an Arrhenius plot of $\ln(\ln(2)/t_{1/2})$ *versus* $1/T$ gives a value of 62(17) kJ mol^{-1} (AC off) (Fig. 3b). This activation energy (with its error margins) compares well to the value of 78 kJ mol^{-1} for the CO release from a CORM-3 analog embedded in a similar alginate@dextran@CORM@IONP composite.[42] Furthermore, we determined the activation energy for the CO release from **1a** to 100(3) kJ mol^{-1}, from **2a** to 96(12) kJ mol^{-1}, from **10** to 99(1) kJ mol^{-1}, from **11** to 96(1) kJ mol^{-1} and from **14** to 111(2) kJ mol^{-1} (see ESI, Fig. S39†). The low correlation for **18** is due to its heterogeneous nature, whereas the CO release from compounds **1a**, **2a**, **10**, **11** and **14** occurred in homogeneous solutions.

Toxicity tests of dextran@oximeCORM@IONP (**17**) against the three cell lines A2780, Cal27 and HEK293 showed no growth inhibition up to a concentration of **17** of 100 μg mL^{-1} (see ESI, Fig. S35–S38†). The three reference compounds CORM-2, CORM-3, and **14** also showed no or low cytotoxic effects with 0–9.23% growth inhibition, respectively, at 10 μmol L^{-1}. A higher concentration of 100 μmol L^{-1} showed moderate growth inhibition of **14** up to 33.9%. For comparison, 100 μmol L^{-1} cisplatin inhibited cell growth by >93% (Table 3).

Conclusions

We have presented the formation of an oxime-based CORM covalently anchored on iron oxide nanoparticles and "solubilized" by a dextran coating. For this, we implemented a synthesis for the immobilization and backbone modification of oxime-based CORMs on iron oxide nanoparticles with a catechol anchor group. A dextran polymer coating with a molar mass of 500 000 g mol^{-1} was applied to achieve good water "solubility" or rather a stable suspension of the modified iron oxide nanoparticles. For the measurement of the CO release with the myoglobin assay, the dark-colored CORM-functionalized iron oxide nanoparticles had to be separated to allow for reliable UV/Vis absorption measurements. This *in situ* separation was achieved by incorporating the "soluble" dextran@oximeCORM@IONP into a calcium alginate sphere. The composite material alginate@dextran@oximeCORM@IONP shows an extended half-life for CO release at 37 °C of 346 ± 83 min compared to the molecular oximeCORMs with the diol-protected catechol backbone **10** of 18 ± ~3 min and the unprotected catechol compound **14** of 16 ± ~1 min in the myoglobin assay. An alternating current magnetic field (31.7 kA m^{-1}, 247 kHz, 39.9 mTesla) leads to a decrease of the half-life at 37 °C from 346 ± 83 (without AC field) to 153 ± 27 (with AC field).

Experimental section

All chemicals were purchased from Acros®, Aldrich®, VWR® and Fluka® and used as received. $[Ru(CO)_3Cl_2]_2$ (**12**) was synthesized according to literature procedures.[48] Doubly-deionized (d.d.) water was obtained by Millipore Synergy with a conductivity of 0.05 μS cm^{-1}.

^{1}H-NMR spectra were recorded with a 300 or 600 MHz Bruker FT-NMR Spectrometer Avance III. For measurements with $CDCl_3$, tetramethylsilane (TMS) was used as an internal reference. Measurements in other solvents were referenced to the solvent signal (DMSO-d_6 2.50 ppm, acetone-d_6 2.04 ppm). All chemical shifts δ are given in ppm. Spectra were recorded at 300 K. ^{1}H and ^{13}C NMR spectra are displayed in Fig. S1a–i in the ESI† and illustrate the purity of the compounds.

Mass spectra were obtained with a HR-MS UHR-QTOF maXis 4G (Bruker Daltonics) or with an ESI Ion-Trap-API-Massenspektrometer Finnigan LCQ Deca (Thermo Quest). Ruthenium-containing fragments show the Ru-96, -98, -99, -100, -101, -102, and -104 isotope distribution patterns. The most intense peak of the isotope distribution is noted in the mass spectrometric assignments (based on ^{102}Ru, mass 101.904 with 31.6% abundancy).

IR spectra were recorded on a Bruker Tensor 37 IR spectrometer as KBr discs or using an attenuated total reflectance (ATR) technique. Care was taken to keep the amount of the nanoparticle composites as low as possible by using only 1–2 mg composite material/30–50 mg KBr because of the strong absorption of the dark nanoparticles. In order to see the relevant carbonyl bands the amount of substance needed to be higher than for pure compounds because of the low ruthenium carbonyl percentage in dextran@oximeCORM@IONP (**17**) and alginate@dextran@oximeCORM@IONP (**18**). Attempted IR spectroscopic measurements of materials containing the black-colored nanoparticles in ATR mode gave only very small signal intensities. Only compounds without nanoparticles were measured by ATR. The integration time was set to 50 scans per wavenumber to obtain good quality spectra. The IR spectra are given in the ESI.†

Dynamic light scattering measurements were carried out with a Malvern Zetasizer Nanoseries. For determination of the nanoparticles size distribution, a dispersion ("solution") with a minimum concentration of 1 mg mL^{-1} in doubly deionized water was prepared. Measurements at different concentrations of the dispersion yielded the same hydrodynamic diameter.

Alternating current (AC) field generator measurements were performed with a Hüttinger HF generator AXIO T5, equipped with a water-cooled copper induction coil. The system was

operated at 247 kHz, with a magnetic field amplitude of 31.7 kA m^{-1} and 39.9 mTesla.

UV/Vis-absorption spectra were collected on a Specord S 600 UV/Vis-spectrometer of Analytik Jena Co. This work was carried out under nitrogen or argon and with thermostated cuvettes.

Atomic absorption spectroscopy (AAS) measurements were performed with a Perkin Elmer AAS AAnalyst200 by MicroLab Kolbe, Höhenweg 17, D-45470 Mülheim.

Transmission electron microscopy (TEM) images were obtained with a Zeiss 902 TEM at the Center for Advanced Imaging (CAi) in the University of Düsseldorf. For the sample preparation about 1 mg of the particles was dispersed by sonication and fast up-and-down pipetting using a 1 mL syringe in deionized water (2 mL). This dispersion was diluted 1 : 10 with deionized water to yield a very low concentration of the nanoparticles. One drop of this dispersion was placed on a holey thin film of amorphous carbon on a copper grid. After a contact time of 15 min, the grid was floated on a water surface and held vertically to rinse of the solvent.

Column chromatography was performed using a Reveleris chromatograph from Grace.

Toxicity tests

Cisplatin was purchased from Sigma-Aldrich, and 3-(4,5-dimethylthiazol-2-yl)-2,5-diphenyltetrazolium bromide (MTT) from Serva (Germany). All other reagents were supplied by PAN Biotech (Germany).

Cell lines and cell culture. The human epithelial ovarian cancer cell line A2780 was obtained from the European Collection of Cell Cultures (ECACC, UK). The human tongue cell line Cal27 and the human embryonic kidney cell line HEK293 were obtained from the German Collection of Microorganisms and Cell Cultures (DSMZ, Germany). All cell lines were grown at 37 °C under a humidified atmosphere containing 5% CO_2 in RPMI 1640 (A2780) or DMEM (Cal27, HEK293) containing 10% fetal calf serum, 120 IU mL^{-1} penicillin, and 120 μg mL^{-1} streptomycin. The cells were grown to 80% confluency before using them for the appropriate assays.

MTT cell viability assay. The rate of cell survival under the action of test compounds was evaluated by an improved MTT assay as previously described.[49] In brief, A2780, Cal27 or HEK293 were seeded at a density of 5000 (A2780) or 2000 (Cal27, HEK293) cells per well in 96-well plates (Corning, Germany). After 24 h, the cells were exposed to increased concentrations of test compounds. Incubation was ended after 72 h and the cell survival was determined by addition of MTT solution (5 mg mL^{-1} in phosphate buffered saline). The formazan precipitate was dissolved in DMSO (VWR, Germany). Absorbance was measured at 544 nm and 690 nm using a FLUOstar microplate reader (BMG LabTech, Germany).

Synthesis

Synthesis of dicarbonylchlorido(imidazole-2-carbaldehydeoxime)(methoxycarbonyl)ruthenium(II) (1a). Solutions of 100 mg (0.20 mmol) of tricarbonyldichloridoruthenium(II)-dimer $[Ru(CO)_3Cl_2]_2$ (**12**) in 1.5 mL of methanol and 66 mg (0.60 mmol) of imidazole-2-carbaldehydeoxime (synthesized according to ref. 50) in another 1.5 mL of methanol were combined and stirred for 5 d at 30 °C. The solution became slightly red and a colorless solid was formed. The solid was separated by centrifugation and washed with cold methanol (3 × 2 mL). Yield: 43 mg (31%, lit.: 41%[38]). IR (KBr): $\tilde{\nu}$ [cm^{-1}] = 2068, 1990. ^{1}H NMR (300 MHz, CD_3OD): δ [ppm] = 8.43 (s, 1H, C–CH═N), 7.42 (s, 1H, imi-CH═CH), 7.37 (s, 1H, imi-CH═CH), 3.36 (s, 3H, CH_3) (matching NMR in ref. 38).

Synthesis of dicarbonylchlorido(imidazol-2-carbaldehydeoxime)(ethoxycarbonyl)ruthenium(II) (2a). 100 mg (0.20 mmol) of tricarbonyldichloridoruthenium(II)-dimer (**12**) were dissolved in 1.5 mL of ethanol. 66 mg (0.60 mmol) of imidazole-2-carbaldehydeoxime (synthesized according to ref. 50) was dissolved in another 1.5 mL of ethanol and subsequently mixed together. The vessel was closed and stirred for 5 d at 30 °C. The solution became slightly red and a colorless solid was formed. The solid was centrifuged and washed with cold ethanol (3 × 2 mL). Yield: 68 mg (45%, lit.: 53%[38]). IR (KBr): $\tilde{\nu}$ [cm^{-1}] = 2067, 1994. ^{1}H NMR (300 MHz, CD_3OD): δ [ppm] = 8.43 (s, 1H, C–CH═N), 7.43 (s, 1H, imi-CH═CH), 7.37 (s, 1H, imi-CH═CH), 3.62 (q, ^3J = 7.1 Hz, 2H, CH_2), 1.20 (t, ^3J = 7.1 Hz, 3H, CH_3) (matching NMR in ref. 38).

Synthesis of 1-(2-(3,4-dihydroxyphenyl)-2-oxoethyl)-1*H*-imidazole-2-carbaldehyde (5). A mixture of 2.0 g (7.0 mmol) of **7** in 200 mL of conc. acetic acid, 66 mL of d.d. water and 26 mL of 6 mol L^{-1} hydrochloric acid was stirred for 2 h at 100 °C. After this the solvent was removed under vacuum, the residue was washed with 80 mL of d.d. water and the solid was removed by centrifugation. The aqueous phase was neutralized with sodium hydroxide, the precipitate was collected by centrifugation and dried under vacuum. Yield: 1.47 g (85%). ESI-MS: m/z = 265.2 $[M + H + H_2O]^+$, 247.2 $[M + H]^+$. ^{1}H NMR (300 MHz, DMSO-d_6): δ [ppm] = 9.64 (d, ^5J = 0.8 Hz, 1H, C–CH═O), 7.56 (t, $^{3/5}J$ = 0.8, 1H, imi-CH═CH), 7.35 (dd, ^3J = 8.4 Hz, ^4J = 2.2 Hz, 1H, C_{aryl}–H), 7.30 (d, ^3J = 0.8 Hz, 1H, imi-CH═CH), 7.25 (d, ^4J = 2.1 Hz, 1H, C_{aryl}–H), 6.65 (d, ^3J = 8.3 Hz, 1H, C_{aryl}–H), 5.88 (s, 2H, C(O)–CH_2–NN). ^{13}C-NMR (see Fig. S1a†) (75 MHz, DMSO-d_6): δ [ppm] = 189.95 (C═O), 181.85 (CH═O), 153.52 (aryl-*C*OH), 146.15 (aryl-*C*OH), 143.51 (N–C═N), 130.82 (aryl-*C*–CO), 128.72 (C_{aryl}–H), 124.99 (imi-CH═CH), 121.52 (imi-CH═CH), 115.35 (C_{aryl}–H), 114.32 (C_{aryl}–H), 53.39 (CH_2).

Synthesis of 2-chloro-1-(2,2-dimethylbenzo[*d*][1,3]dioxol-5-yl) ethanone (6). A mixture of 6.0 g (32.6 mmol) of 2-chloro-2,4-dihydroxy-acetophenone with 0.95 g phosphorus pentoxide in 120 mL of dry toluene was stirred under nitrogen at 75 °C and, every 20 min a portion of 0.55 mL acetone and every 30 min 0.85 g phosphorus pentoxide were added over a period of 4 h. After adding 24 mL of aqueous 20% sodium hydroxide, the aqueous phase was removed by decantation and discarded. The organic phase was washed with d.d. water (3 × 60 mL). The toluene solvent was removed and the solid was dried under vacuum. Yield: 6.6 g (87%). ^{1}H NMR (see Fig. S1b†) (300 MHz, acetone-d_6): δ [ppm] = 7.64 (dd, ^3J = 8.2 Hz, ^4J = 1.8

Hz, 1H, C_{aryl}–H), 7.37 (dd, ^4J = 1.8 Hz, ^5J = 0.4 Hz, 1H, C_{aryl}–H), 6.90 (dd, ^3J = 8.2 Hz, ^5J = 0.4 Hz, 1H, C_{aryl}–H), 4.91 (s, 2H, CH_2–Cl), 1.71 (s, 6H, CH_3).

Synthesis of 1-(2-(2,2-dimethylbenzo[*d*][1,3]dioxol-5-yl)-2-oxoethyl)-1*H*-imidazole-2-carbaldehyde (7). 5.0 g (22.1 mmol) of **6**, 2.34 g (22.1 mmol) Na_2CO_3 and 4.24 g (44.2 mmol) imidazole-2-carboxaldehyde (**4**) were dissolved in 200 mL of acetonitrile and stirred for 10 d at 60 °C under a dry atmosphere. The solid was removed by centrifugation and the supernatant solution was poured into 1 L of d.d. water. The formed solid was separated by centrifugation and dried under vacuum. The crude product was dissolved in 60 mL of ethyl acetate and purified using a Reveleris Chromatograph from Grace (4 runs with 120 g silica column, ethyl acetate 40 mL min^{-1}). Yield: 2.5 g (40%). ^{1}H NMR (Fig. S1c†) (300 MHz, acetone-d_6): δ [ppm] = 9.67 (d, ^5J = 0.9 Hz, 1H, C–CH=O), 7.71 (dd, ^3J = 8.2 Hz, ^4J = 1.8 Hz, 1H, C_{aryl}–H), 7.48 (t, $^{3/5}J$ = 0.9 Hz, 1H, imi-CH=CH), 7.40 (d, ^4J = 1.8 Hz, 1H, C_{aryl}–H), 7.30 (d, ^3J = 0.9 Hz, 1H, imi-CH=CH), 6.94 (d, ^3J = 8.1 Hz, 1H, C_{aryl}–H), 5.99 (s, 2H, C(O)–CH_2–N), 1.72 (s, 6H, CH_3). ^{13}C NMR (Fig. S1d†) (75 MHz, acetone-d_6): δ [ppm] = 190.56 (C=O), 182.61 (CH=O), 153.11 (aryl-*C*OH), 148.99 (aryl-*C*OH), 144.84 (N–C=N), 131.82 (aryl-*C*–CO), 129.79 (C_{aryl}–H), 129.02 (imi-CH=CH), 124.87 (imi-CH=CH), 120.67 (*C*-$(CH_3)_2$), 108.89 (C_{aryl}–H), 108.04 (C_{aryl}–H), 54.33 (CH_2), 25.89 (CH_3).

Synthesis of (*E*)-1-(2-(2,2-dimethylbenzo[*d*][1,3]dioxol-5-yl)-2-oxoethyl)-1*H*-imidazol-2-carbaldehyde-oxime (8). A mixture of 200 mg (0.70 mmol) of **7** with 74 mg (0.7 mmol) of sodium carbonate and 94 mg (1.4 mmol) of hydroxyl ammonium chloride, $[NH_3OH]Cl$ in 4 mL of d.d. water was stirred for 24 h at 70 °C. The obtained solid was separated by centrifugation at 5 °C, washed with ethyl acetate (3 × 5 mL) and dried under vacuum. Yield: 158 mg (75%). ESI-MS: *m*/*z* = 302.1 $[M + H]^+$. ^{1}H NMR (Fig. S1e†) (300 MHz, DMSO-d_6): δ [ppm] = 11.22 (s, 1H, NO–H), 7.97 (s, 1H, C–CH=N), 7.65 (dd, ^3J = 8.2 Hz, ^4J = 2.4 Hz, 1H, C_{aryl}–H), 7.44 (d, ^4J = 1.7 Hz, 1H, C_{aryl}–H), 7.24 (d, ^3J = 0.9 Hz, 1H, imi-CH=CH), 7.04 (d, ^3J = 1 Hz, 1H, imi-CH=CH), 7.02 (d, ^3J = 8.35 Hz, 1H, C_{aryl}–H), 5.86 (s, 2H, C(O)–CH_2–N), 1.70 (s, 6H, CH_3).

Synthesis of 1-(2-(3,4-dihydroxyphenyl)-2-oxoethyl)-1*H*-imidazole-2-carbaldehyde-oxime (9). 300 mg (1.22 mmol) of **5**, 95 mg (1.22 mmol) of Na_2CO_3 and 169 mg (2.44 mmol) of hydroxyl ammonium chloride were dissolved in 10 mL of d.d. water and stirred for 24 h at 70 °C. The solid was separated by centrifugation at 5 °C, washed with d.d. water (3 × 5 mL) and dried under vacuum. Yield: 151 mg (47%). IR (KBr): $\tilde{\nu}$ [cm^{-1}] = 1692, 1472. High-resolution, HR-ESI MS: *m*/*z* = 262.0822, calc. for $[M + H]^+$ *m*/*z* = 262.0823, matching with the exact mass for the indicated fragment; the absence of other significant peaks (besides the isotope pattern) confirms the purity of compound **9** (see Fig. S4a†). ^{1}H-NMR (Fig. S1f†) (600 MHz, DMSO-d_6): δ [ppm] = 11.21 (s, 1H, N–OH), 9.99 (s, 1H, C–OH), 9.45 (s, 1H, C–OH), 7.96 (s, 1H, C–CH=N), 7.44 (dd, ^3J = 8.27 Hz, ^4J = 2.1 Hz, 1H, C_{aryl}–H), 7.37 (d, ^4J = 2.1 Hz, 1H, C_{aryl}–H), 7.23 (s br, 1H, imi-CH=CH), 7.03 (s br, 1H, imi-CH=CH), 6.87 (d, ^3J = 8.26, C_{aryl}–H), 5.80 (s, 2H, C(O)–CH_2–N). ^{13}C-NMR (Fig. S1g†) (125 MHz, DMSO-d_6): δ [ppm] = 190.62 (C=O), 151.22 (aryl-*C*OH), 145.37 (aryl-*C*OH), 141.44 (CH=NOH), 140.41 (s, 1C, N–C=N), 128.34 (aryl-*C*–CO), 126.30 (C_{aryl}–H), 124.77 (imi-CH=CH), 121.14 (imi-CH=CH), 115.20 (C_{aryl}–H), 114.69 (C_{aryl}–H), 53.33 (CH_2).

Synthesis of [Ru(η^2-8)(methoxycarbonyl)(CO)$_2$Cl] (10). 270 mg (0.9 mmol) of **8** and 170 mg (0.3 mmol) of $[Ru(CO)_3Cl_2]_2$ (**12**) were separately dissolved in 2.5 mL of methanol, combined and stirred for 5 d at 30 °C in a closed vessel. The solid was sedimented by centrifugation at 5 °C, washed with cold methanol (3 × 5 mL) and dried under vacuum. Yield: 249 mg (50%). IR (ATR): $\tilde{\nu}$ [cm^{-1}] = 2074; 1985, IR (KBr): $\tilde{\nu}$ [cm^{-1}] = 2075; 1989. ESI-MS: *m*/*z* = 527.0 $[M - OMe^- - Cl^- - H^+ + CH_3CN]^+$, 499.1 $[M - CO/OMe^- - Cl^- - H^+ + CH_3CN]^+$. ^{1}H NMR (Fig. S1h†) (300 MHz, acetone-d_6): δ [ppm] = 8.75 ("d" = 2s for different *cis*- and *trans* ligands, 1H, C–CH=N), 7.72 (dd, ^3J = 8.2, 1.8 Hz, 1H, C_{aryl}–H), 7.51–7.46 (m, 2H, imi-CH=CH), 7.42 (d, ^4J = 1.8 Hz, 1H, C_{aryl}–H), 6.97 (d, ^3J = 8.2 Hz, 1H, C_{aryl}–H), 6.05 (s br, 2H, C(O)–CH_2–N), 3.75 (s, 3H, $COOCH_3$), 1.72 (s, 6H, $(CH_3)_2$).

Synthesis of [Ru(η^2-8)(ethoxycarbonyl)(CO)$_2$Cl] (11). 250 mg (0.83 mmol) of **8** and 160 mg (0.313 mmol) of $[Ru(CO)_3Cl_2]_2$ (**12**) were separately dissolved in 2.5 mL of ethanol, combined and stirred for 5 d at 30 °C in a closed vessel. The solid was sedimented by centrifugation at 5 °C, washed with cold ethanol (3 × 5 mL) and dried under vacuum. Yield: 221 mg (47%). IR (ATR): $\tilde{\nu}$ [cm^{-1}] = 2059; 1986, IR (KBr): $\tilde{\nu}$ [cm^{-1}] = 2065, 1988. ESI-MS (Fig. S3a†): *m*/*z* = 527.0 $[M - OEt^- - Cl^- - H^+ + CH_3CN]^+$, 499.1 $[M - CO/OEt^- - Cl^- - H^+ + CH_3CN]^+$. ^{1}H NMR (Fig. S1i†) (300 MHz, acetone-d_6): δ [ppm] = 8.73 ("d" = 2s for different *cis*- and *trans* ligands, 1H, C–CH=N), 7.72 (dd, ^3J = 8.2 Hz, ^4J = 1.8 Hz, 1H, C_{aryl}–H), 7.51–7.47 (m, 2H, imi-CH=CH), 7.42 (d, ^4J = 1.8 Hz, 1H, C_{aryl}–H), 6.97 (d, ^3J = 8.2 Hz, 1H, C_{aryl}–H), 6.06 (s br, 2H, C(O)–CH_2–N), 4.26 (t, ^3J = 8 Hz, 2H, –OCH_2–), 1.72 (s, 6H, $C(CH_3)_2$), 1.28 (t, ^3J = 7 Hz, 3H, –CH_3).

Synthesis of [Ru(η^2-9)(methoxycarbonyl)(CO)$_2$Cl] (13). 50 mg (0.19 mmol) of **9** and 48 mg (96 μmol) of $[Ru(CO)_3Cl_2]_2$ (**12**) were separately dissolved in 1 mL of methanol, combined and stirred for 5 d at 30 °C in a closed vessel. The solvent was removed under vacuum and the solid was analysed as a crude product. Compound **13**, which was detected by mass spectrometric analysis, did not precipitate in a concentrated or cold solution and we were not able to purify the crude product. Therefore, compound **14** which could be precipitated from the solution as a colorless product and purified with cold ethanol was used for the CO release experiments. Yield: 88.5 mg (crude product). ESI-MS: *m*/*z* = 487.0 $[M - OMe^- - Cl^- - H^+ + CH_3CN]^+$, 459.2 $[M - CO/OMe^- - Cl^- - H^+ + CH_3CN]^+$.

Synthesis of [Ru(η^2-9)(ethoxycarbonyl)(CO)$_2$Cl] (14). 50 mg (0.19 mmol) **9** and 32 mg **12** (63 μmol) were separately dissolved in 1 mL ethanol, combined and stirred for 5 d at 30 °C in a closed vessel. The solid was sedimented by centrifugation at 5 °C, washed with cold ethanol (3 × 5 mL) and dried under vacuum. Yield: 70 mg (70%). IR (KBr): $\tilde{\nu}$ [cm^{-1}] = 2064, 1995, 1678, 1478. ESI-MS (Fig. S3b†): *m*/*z* = 487.0 $[M - OEt^- - Cl^-$ –

$H^+ + CH_3CN]^+$, 459.1 [M − CO/OEt$^-$ − Cl$^-$ − $H^+ + CH_3CN]^+$. High-resolution, HR-ESI-MS: *m*/*z* = 486.9828 [M − OEt$^-$ − Cl$^-$ − $H^+ + CH_3CN]^+$, 458.9877 [M − CO/OEt$^-$ − Cl$^-$ − $H^+ + CH_3CN]^+$, 419.9768 [M − CO/OEt$^-$ − Cl$^\bullet$ + H]$^+$, all matching with the calculated patterns for the indicated fragment masses (see Fig. S4b–d†). ^{1}H NMR (500 MHz, acetone-d_6): δ [ppm] = 8.70 (s, 1H, C-CH═N), 7.60–7.38 (m, 4H, imi-CH═CH, 2C_{aryl}–H), 6.99 (d, ^3J = 8.2, 1H, C_{aryl}–H), 6.11–5.88 (m, 2H, C(O)–CH_2–N), 3.57 (q, ^3J = 6.5, 2H, –OCH_2–), 1.12 (t, ^3J = 6.7, 3H, –CH_3). Calcd for $C_{17}H_{16}ClN_3O_8Ru$ (526.85 g mol^{-1}): C 38.76, H 3.06, N 7.98, found: C 38.72, H 3.09, N 7.47%.

Immobilization of 14 on maghemite nanoparticles (16). A suspension of 5 mg of **14** in 2 mL of d.d. water was mixed with a few drops of 0.1 mol L^{-1} sodium hydroxide to form a clear solution. 30 mg of maghemite nanoparticles (**15**) were added as an aqueous dispersion (3 mL, 10 mg mL^{-1}) and the solution was stirred for 15 min. To prevent agglomeration of the nanoparticles the combined solutions of both compounds were kept below pH 8. After neutralizing with hydrochloric acid the solution was combined with 100 mL acetone and the precipitated solid was removed by centrifugation. The solid was washed with ethanol 3 × 5 mL and dried under vacuum. Yield: 27 mg, IR (KBr): $\tilde{\nu}$ [cm^{-1}] = 2038, 1916, 1633, 1487.

Immobilization of 14 on maghemite nanoparticles in dextran (17). A suspension of 5 mg of **14** in 2 mL of d.d. water was mixed with a few drops of 0.1 mol L^{-1} sodium hydroxide to form a clear solution. 30 mg of maghemite nanoparticles (**15**) were added as an aqueous dispersion (3 mL, 10 mg mL^{-1}) and the solution was stirred for 15 min. Separately 60 mg dextran (M = 500 000 g mol^{-1}) was dissolved in 5 mL of d.d. water, combined with the above solution and stirred for 3 h. After neutralizing with hydrochloric acid, 100 mL of acetone were added and the formed solid removed by centrifugation. The solid was washed with ethanol 3 × 5 mL and the brown solid, now called composite material dextran@oximeCORM@IONP (**17**) was dried under vacuum and stored for several weeks. Yield: 69 mg, IR (KBr): $\tilde{\nu}$ [cm^{-1}] = 2064, 1995, 1961.

Embedding of 17 into alginate spheres (18). 10 mg of **17** were dissolved in 0.5 mL MOPS buffer (pH 7.4). Mixing of 0.5 mL of this solution with 0.5 mL alginate solution (50 mg sodium alginate in 10 mL d.d. water) leads to a viscous solution which was added dropwise (by B-Braun, Sterican syringe with a 0.60 × 80 mm BL/LB needle) into a calcium chloride solution (2 g $CaCl_2 \cdot 6H_2O$ in 60 mL of d.d. water). The resulting spheres were left to stand for 30 min in the calcium chloride solution to form a fully cross-linked network of the alginate. Then the formed spheres were washed three times each with 10 mL of MOPS buffer and used directly for kinetic CO release experiments with the myoglobin assay.

CO detection

MOPS buffer 0.1 mol L^{-1} pH 7.4. 2.09 g (0.01 mol) of 3-(*N*-morpholino)propanesulfonic acid (MOPS) were dissolved in 75 mL of d.d. water. Subsequently, the pH was adjusted to 7.4 using NaOH and water was added to reach a final volume of 100 mL.

Myoglobin assay with molecular, soluble oxime-based CORMs. Myoglobin from equine skeletal muscle (6.3 mg) was dissolved in 5 mL 3-(*N*-morpholino)propanesulfonic acid buffer (pH 7.4; 0.1 mol L^{-1}) and deoxygenated for 10 min with nitrogen to yield a myoglobin solution (66 μmol L^{-1}). Solid sodium dithionite was added (5 mg) to fully reduce the myoglobin to the Fe(II) state and the solution was deoxygenated with nitrogen for an additional 10 min. To receive a 10 mmol L^{-1} solution of the CORM, 1 mg of the compound was dissolved in a corresponding amount of dimethylsulfoxide. A thermostable quartz-cell was filled with 1.5 mL myoglobin solution and 6 μL of the CORM-solution and sealed with a Teflon plug to start the measurement immediately.

Myoglobin assay with alginate@dextran@oximeCORM@IONP. A thermostable quartz-cell was filled with 1.3 mL MOPS buffer solution, 15 spheres of alginate@dextran@oximeCORM@IONP (**18**), 200 μL of the above myoglobin/MOPS/$Na_2S_2O_3$ solution and sealed with a Teflon plug to start the UV/Vis measurement immediately.

CO release in alternating current (AC) field. Measurements were performed with a Hüttinger HF generator AXIO T5, equipped with a water-cooled copper induction coil. The system was operated at 247 kHz, with a magnetic field amplitude of 31.7 kA m^{-1} and 39.9 mTesla. The thermostated quartz-cell was placed inside the copper induction coil (see Fig. S40 in the ESI†). To keep the alginate spheres on the bottom of the UV-cell, a small permanent magnet was placed under the quartz-cell. In order to keep the conditions reproducible, this permanent magnet was used during every measurement, even without alginate.

Acknowledgements

We thank Dr Juri Barthel and the Ernst Ruska-Centre (ER-C) for Microscopy and Spectroscopy with Electrons, the Jülich Research Centre and the RWTH Aachen University, 52425 Jülich (Germany) for help and access to the HR-TEM facilities. Dr Peter Tommes is thanked for collecting the HR-ESI mass spectra.

Notes and references

1 B. J. Haldane, *Biochem. J.*, 1927, **21**, 1068–1075.
2 L. D. Prockop and R. I. Chichkova, *J. Neurol. Sci.*, 2007, **262**, 122–130.
3 T. R. Johnson, B. E. Mann, J. E. Clark, R. Foresti, C. J. Green and R. Motterlini, *Angew. Chem., Int. Ed.*, 2003, **42**, 3722–3729.
4 A. W. Carpenter and M. H. Schoenfisch, *Chem. Soc. Rev.*, 2012, **41**, 3742–3752.
5 D. S. Bredt and S. H. Snyder, *Annu. Rev. Biochem.*, 1994, **63**, 175–195.
6 B. E. Mann and R. Motterlini, *Chem. Commun.*, 2007, 4197–4208.

7 R. Tenhunen, H. S. Marver and R. Schmid, *Proc. Natl. Acad. Sci. U. S. A.*, 1968, **61**, 748–755.
8 D. Boehning and S. H. Snyder, *Science*, 2002, **298**, 2339–2340.
9 R. Motterlini and L. E. Otterbein, *Nature*, 2010, **9**, 728–743.
10 B. E. Mann, *Organometallics*, 2012, **31**, 5728–5735.
11 R. Motterlini and L. E. Otterbein, *Nat. Rev. Drug Discovery*, 2010, **9**, 728–743.
12 R. Foresti and R. Motterlini, *Curr. Drug Targets*, 2010, **11**, 1595–1604.
13 M. Patra, M. Wenzel, P. Prochnow, V. Pierroz, G. Gasser, J. E. Bandow and N. Metzler-Nolte, *Chem. Sci.*, 2015, **6**, 214–224.
14 R. Motterlini, J. E. Clark, R. Foresti, P. Sarathchandra, B. E. Mann and C. J. Green, *Circ. Res.*, 2002, **90**, 17–24.
15 R. Motterlini, B. E. Mann, T. R. Johnson, J. E. Clark, R. Foresti and C. J. Green, *Curr. Pharm. Des.*, 2003, **9**, 2525–2539.
16 J. E. Clark, P. Naughton, S. Shurey, C. J. Green, T. R. Johnson, B. E. Mann, R. Foresti and R. Motterlini, *Circ. Res.*, 2003, **93**, 2–8.
17 R. Alberto and R. Motterlini, *Dalton Trans.*, 2007, 1651–1660.
18 R. Motterlini, B. E. Mann and R. Foresti, *Expert Opin. Invest. Drugs*, 2005, **14**, 1305–1318.
19 S. McLean, B. E. Mann and R. K. Poole, *Anal. Biochem.*, 2012, **427**, 36–40.
20 T. R. Johnson, B. E. Mann, I. P. Teasdale, H. Adams, R. Foresti and C. J. Green, *Dalton Trans.*, 2007, 1500–1508.
21 T. Santos-Silva, A. Mukhopadhyay, J. D. Seixas, G. J. L. Bernandes, C. C. Romao and M. J. Romao, *J. Am. Chem. Soc.*, 2011, **133**, 1192–1195.
22 T. Pitchumony, B. Spingler, R. Motterlini and R. Alberto, *Chimia*, 2009, **62**, 277–279.
23 R. Motterlini, P. Sawle, J. Hammad, S. Bains, R. Alberto, R. Foresti and C. J. Green, *FASEB J.*, 2005, **19**, 284–286.
24 N. E. Brückmann, M. Wahl, G. J. Reiß, M. Kohns, W. Wätjen and P. C. Kunz, *Eur. J. Inorg. Chem.*, 2011, 4571–4577.
25 W. Huber, R. Linder, J. Niesel, U. Schatzschneider, B. Spingler and P. C. Kunz, *Eur. J. Inorg. Chem.*, 2012, 3140–3146.
26 S. Romanski, B. Kraus, U. Schatzschneider, J. M. Neudörfl, S. Amslinger and H. G. Schmalz, *Angew. Chem., Int. Ed.*, 2011, **50**, 2392–22396.
27 N. S. Sitnikov, Y. Li, D. Zhang, B. Yard and H.-G. Schmalz, *Angew. Chem., Int. Ed.*, 2015, **54**, 12314–12318.
28 M. Ma, H. Noei, B. Mienert, J. Niesel, E. Bill and M. Muhler, *Chem. – Eur. J.*, 2013, **19**, 6785–6790.
29 G. Dördelmann, T. Meinhardt, T. Sowik, A. Krüger and U. Schatzschneider, *Chem. Commun.*, 2012, **48**, 11528–11530.
30 A. Ruggi and F. Zobi, *Dalton Trans.*, 2015, **44**, 10928–10931.
31 C. Bohlender, S. Glaeser, M. Klein, J. Weisser, S. Thein, U. Neugebauer, J. Popp, R. Wyrwa and A. J. Schiller, *J. Mater. Chem. B*, 2014, **2**, 1454–1463.
32 U. Schatzschneider, *Br. J. Pharmacol.*, 2015, **172**, 1638–1650.
33 Y. Matsumura and H. Maeda, *Cancer Res.*, 1986, **46**, 6387–6392.
34 H. Maeda, J. Wu, T. Sawa, Y. Matsumura and K. Hori, *J. Controlled Release*, 2000, **65**, 271–284.
35 L. D. D'Andrea, A. Romanelli, R. Di Stasi and C. Pedone, *Dalton Trans.*, 2010, **39**, 7625–7636.
36 E. Neuse, *Met.-Based Drugs*, 2008, 1–19.
37 J. D. Seixas, F. A. Marino, A. Mukhopadhyay, A. C. Coelho, P. M. Reis, L. F. Veiros, A. R. Marques, N. Penacho, A. M. L. Goncalves, M. J. Romao, G. J. L. Bernardes, T. Santos-Silva and C. C. Romao, *Dalton Trans.*, 2015, **44**, 5058–5075.
38 L. Oresmaa, H. Tarvainen, K. Machal and M. Haukka, *Dalton Trans.*, 2012, **41**, 11170–11175.
39 P. C. Kunz, H. Meyer, J. Barthel, S. Sollazzo, A. M. Schmidt and C. Janiak, *Chem. Commun.*, 2013, **49**, 4896–4898.
40 B. F. G. Johnson and J. S. McIndoe, *Coord. Chem. Rev.*, 2000, **200–202**, 901–932.
41 G. A. van Ewijk, G. J. Vroege and A. P. J. Philip, *J. Magn. Magn. Mater.*, 1999, **201**, 31–33.
42 H. Meyer, F. Winkler, P. Kunz, A. M. Schmidt, A. Hamacher, M. U. Kassack and C. Janiak, *Inorg. Chem.*, 2015, **54**(23), 11236–11246.
43 M. Klein, U. Neugebauer, A. Gheisari, A. Malassa, T. M. Jazzazi, F. Froehlich, M. Westerhausen, M. Schmitt and J. Popp, *J. Phys. Chem. A*, 2014, **118**, 5381–5390.
44 L. Yuan, W. Y. Lin, L. Tan, K. B. Zheng and W. M. Huang, *Angew. Chem., Int. Ed.*, 2013, **52**, 1628–1630.
45 B. W. Michel, A. R. Lippert and C. J. Chang, *J. Am. Chem. Soc.*, 2012, **134**, 15668–15671.
46 H. J. Vreman and D. K. Stevenson, *Anal. Biochem.*, 1988, **168**, 31–81.
47 M. Balazy and H. Jiang, *Acta Haematol.*, 2000, **103**, 78–83.
48 A. Mantovani and S. Cenini, *Inorg. Synth.*, 1976, **16**, 51–53.
49 L. Marek, A. Hamacher, F. K. Hansen, K. Kuna, H. Gohlke, M. U. Kassack and T. Kurz, *J. Med. Chem.*, 2013, **56**, 427–436.
50 L. Oresmaa, H. Kotikoski, M. Haukka, J. Salminen, O. Oksala, E. Pohjala, E. Moilanen, H. Vapaatalo, P. Vainiotalo and P. Aulaskari, *J. Med. Chem.*, 2005, **48**, 4231–4236.